ANNUAL REVIEWS

Annual Review of Biochemistry

Biological Insight from Super-Resolution Microscopy: What We Can Learn from Localization-Based Images

David Baddeley[1,2] and Joerg Bewersdorf[1,3]

[1]Department of Cell Biology, Yale School of Medicine, New Haven, Connecticut 06520, USA; email: d.baddeley@auckland.ac.nz, joerg.bewersdorf@yale.edu

[2]Auckland Bioengineering Institute, University of Auckland, Auckland 1010, New Zealand

[3]Department of Biomedical Engineering, Yale University, New Haven, Connecticut 06520, USA

Annu. Rev. Biochem. 2018. 87:965–89

First published as a Review in Advance on December 22, 2017

The *Annual Review of Biochemistry* is online at biochem.annualreviews.org

https://doi.org/10.1146/annurev-biochem-060815-014801

Keywords

single-molecule localization microscopy, nanoscopy, quantitative analysis, PALM, STORM, PAINT

Abstract

Super-resolution optical imaging based on the switching and localization of individual fluorescent molecules [photoactivated localization microscopy (PALM), stochastic optical reconstruction microscopy (STORM), etc.] has evolved remarkably over the last decade. Originally driven by pushing technological limits, it has become a tool of biological discovery. The initial demand for impressive pictures showing well-studied biological structures has been replaced by a need for quantitative, reliable data providing dependable evidence for specific unresolved biological hypotheses. In this review, we highlight applications that showcase this development, identify the features that led to their success, and discuss remaining challenges and difficulties. In this context, we consider the complex topic of defining resolution for this imaging modality and address some of the more common analytical methods used with this data.

Contents

1. INTRODUCTION

Optical nanoscopy: diffraction-unlimited super-resolution microscopy including SMLM as well as STED and RESOLFT approaches

Resolution: capability of a microscope to distinguish two neighboring objects

Localization: short for "localization event"; an individual single-molecule detection and position determination carried out by computational postprocessing of acquired images

With the 2014 Nobel Prize in Chemistry, if not before, (optical) super-resolution microscopy became a central tool in the biomedical research community (1). Super-resolution microscopy, or optical nanoscopy, encompasses a variety of techniques that improve the resolution of lens-based (far-field) fluorescence microscopes beyond the diffraction limit (approximately 250 nm in the focal plane and 500–700 nm in the depth direction). Super-resolution microscopy techniques can be sorted into two groups: The first group, which includes structured illumination microscopy and derivatives (2–4), exploits wave optics and image processing to push diffraction to its ultimate limit; the second group, which includes STED (STimulated Emission Depletion) microscopy (5, 6), other members of the RESOLFT (REversible Saturable or switchable OpticaL Fluorescence Transitions) family (7), and SOFI (Stochastic Optical Fluctuation Imaging) (8) as well as the single-molecule switching and localization techniques discussed in this review, breaks the diffraction limit by taking advantage of turning fluorescent markers on and off (often in combination with techniques of the first group) (9).

Many of these techniques have matured from a proof-of-concept stage to commercial instruments over the last two decades, and the number of super-resolution microscopes worldwide is approaching the thousands. Many excellent review articles have been written about super-resolution microscopy, and we refer to these for an introduction and overview on the topic (9–13). More recently, the field has focused on consolidating many of the pioneering development efforts of the early years. Especially in the single-molecule switching and localization field (PALM, STORM, FPALM, and related techniques), extracting meaningful information in a reliable and

reproducible way has lately become the subject of many debates and articles. This article reviews and reflects on some of the limitations and underlying concepts that have triggered these discussions.

1.1. Working Principle of Single-Molecule Switching and Localization Nanoscopy

Single-molecule switching and localization nanoscopy generates super-resolved images by determining the spatial position of large numbers of individual fluorescent molecules that label a structure. In conventional fluorescence microscopes, most illuminated probe molecules emit fluorescence at the same time. Diffraction causes each fluorescent molecule to appear as a spot of at least ~250 nm in size, as described by the point-spread function (PSF). Molecules closer than this spot size overlap and cannot be readily distinguished from each other.

By switching on only a small, random subpopulation of molecules in each recorded camera frame, the density of emitting molecules can (ideally) be lowered to the point at which the images of neighboring fluorescent emitters do not overlap and each individual emitter can be isolated and its location determined with subdiffraction precision (see Section 4.1). By imaging them in separate camera frames, two molecules, which would be too close together to be distinguishable using conventional microscopy, can be resolved. To acquire the locations of enough molecules to form a sufficiently detailed image (see Section 4.2), many frames, typically thousands to hundreds of thousands, are recorded, each showing a different subpopulation of molecules that "blink" or "flash."

These flashes are usually produced by switching molecules between visible and invisible states. "On" switching is most frequently achieved by actively turning on random subsets of photoswitchable molecules with light or by passively watching molecules that have previously been pumped to the invisible state spontaneously switch back to the visible state. "Off" switching is usually realized by either permanently or temporarily bleaching visible molecules with the light that is also used to read out the fluorescence. These approaches are known under the acronyms PALM (photoactivated localization microscopy), STORM (stochastic optical reconstruction microscopy), FPALM (fluorescence photoactivation localization microscopy), dSTORM (direct stochastic optical reconstruction microscopy), GSDIM (ground state depletion with individual molecule return), and many others (14–20). Alternatively, chemical binding kinetics can be exploited. Here, diffusing fluorescent probe molecules are not visible because their rapid motion blurs the signal and they do not produce spot-like intensity patterns. As soon as they bind to a target molecule, however, they become immobile and are thereby visible until they are bleached (or become mobile again). This approach, known under the acronym PAINT (points accumulation for imaging in nanoscale topography) (21), can be further refined by using fluorogenic probe molecules that become fluorescent only upon binding and by optimizing the time that ligands bind reversibly (22–27).

Regardless of the switching mechanism used, these approaches have the common property that individual single molecules are detected and their positions accurately measured using computational postprocessing. Throughout this review, we refer to an individual single-molecule detection and position determination as a localization event, or in short, localization. In reference to the importance of these localizations, especially with respect to the quantitative data analysis emphasized in this article, we have adopted the commonly used term of single-molecule localization microscopy (SMLM) throughout this review, even though there are good arguments that stochastic switching is conceptually more fundamental to the understanding of how the diffraction limit is overcome (28).

Point-spread function (PSF): describes the appearance of a point-like object when viewed with a microscope

Single-molecule localization microscopy (SMLM): commonly used term for super-resolution techniques relying on "on" and "off" switching of individual molecules and their localization

1.2. Applied Quantitative Single-Molecule Localization Microscopy

Localization density: number of localizations per unit length, area, or volume

From a biological perspective, applications to date can be broadly classified into two major categories: visualizing structures and investigating interactions. Although this division is somewhat arbitrary and inexact, with some applications clearly spanning both categories, we believe it is instructive as these two tasks place fundamentally different demands on the imaging modality. In the next two sections, we build on this categorization to take an application-centric look at what is necessary to get good quantitative super-resolution data in a variety of scenarios.

2. IMAGING STRUCTURES

Structural super-resolution imaging is directly analogous to electron microscopy, albeit with specific molecular contrast, by having interest in the shape and/or arrangement of a particular functional structure within the cell. In structural imaging, one typically derives most of the information from a single label or color channel, although additional channels may provide valuable contextual information. The difficulty of the imaging and data interpretation tasks can vary dramatically. For illustration, we have broken down structural super-resolution imaging into subcategories of increasing difficulty (**Figure 1**).

2.1. Well-Isolated Repetitive and/or Stereotyped Structures

Many of the most biologically meaningful results published to date have been well-isolated, repetitive, and/or stereotyped structures. One of the most striking examples is the spectacular discovery of periodic actin rings in neuronal axons by Xu and colleagues (29) in 2013 and the subsequent quantification of the spacing and demonstration that this was consistent with a spectrin scaffold (**Figure 2*a***). The regular spacing between the observed actin rings and their similarity led to a strikingly clear and compelling result. Sperm flagella lend themselves to a comparable approach. The uniform shape of the flagellum allows the flagellum to be treated as a cylinder and the localizations to be projected in the direction of the cylinder axis, thereby obtaining images depicting the radial/azimuthal protein distribution at high quality (30).

Another example is the characterization of the y-complex in nuclear pore complexes (NPCs) (31), which builds on the demonstration that the stereotyped nature of the NPC allows averaging of a high number of spatially aligned NPC images to produce a well-sampled composite (32, 33). Szymborska et al. (31) applied this approach to seven subunits of the y-complex and were able to resolve their relative radial positions and deduce the overall y-complex orientation within the NPC (**Figure 2*b***). A similar approach has been used to investigate the ciliary transition zone architecture (34) and to reconstruct the icosahedral shape of T7 bacteriophages from SMLM data sets of individual capsids (35).

The idea of stereotyping and population averaging can be expanded to structures such as gene loci even though, at a first glance, they do not seem to resemble one another. By choosing a metric that extracts stereotypical features within the population (e.g., the radius of gyration), very useful properties such as the average level of compaction of a certain type of gene locus can be determined (36) (**Figure 2*c***). A similar logic, taking the population average of a simplifying metric, has allowed the size of cytokinesis nodes in yeast (37) to be estimated along with a growing number of additional applications.

While all these examples take advantage of, and indeed rely on, good localization accuracy, the similarity of individual structures allows the information from multiple structures to be combined, relaxing the demands on labeling and localization density. However, there is a necessary prerequisite: If information from multiple structures is to be combined, the structures must also

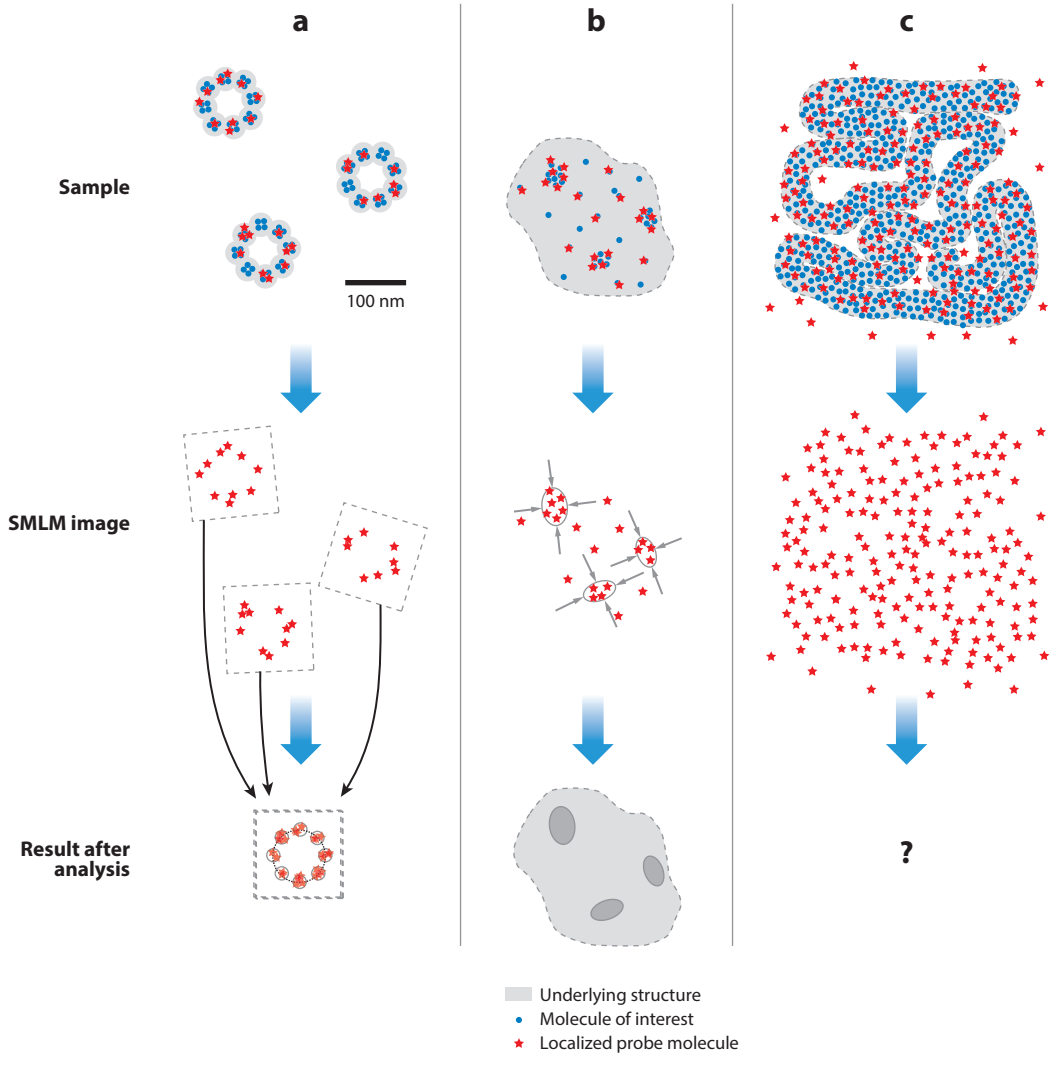

Figure 1

For the purposes of this review, we separate biological structures into three classes: (*a*) structures that are well separated, are highly similar, and can be averaged (e.g., nuclear pore complexes), (*b*) structures that are still well separated but do not possess a high degree of similarity and must be analyzed individually (e.g., proteins in the active zone of synapses), and (*c*) structures that are highly complex and not well separated (e.g., condensed chromatin). In each case, molecules of interest (*blue dots*) are detected with less than 100% efficiency leading to imperfect localization data (*stars*). Abbreviation: SMLM, single-molecule localization microscopy.

be easily identifiable and isolated from their surroundings. This implies both a reasonable amount of separation between individual structures and low levels of background (whether from unspecific labeling, cytoplasmic pools, or out-of-focus structures).

Biological studies that can exploit these criteria of isolation and the ability to be averaged—either through the intrinsic nature of the structure studied or by careful choice of experimental conditions and metrics—lend themselves to the generation of robust quantitative results despite limitations on labeling efficiencies inherent to the current state of the art. Not surprisingly, the most impactful publications to date tend to fall into this category. Saying that these are the easiest

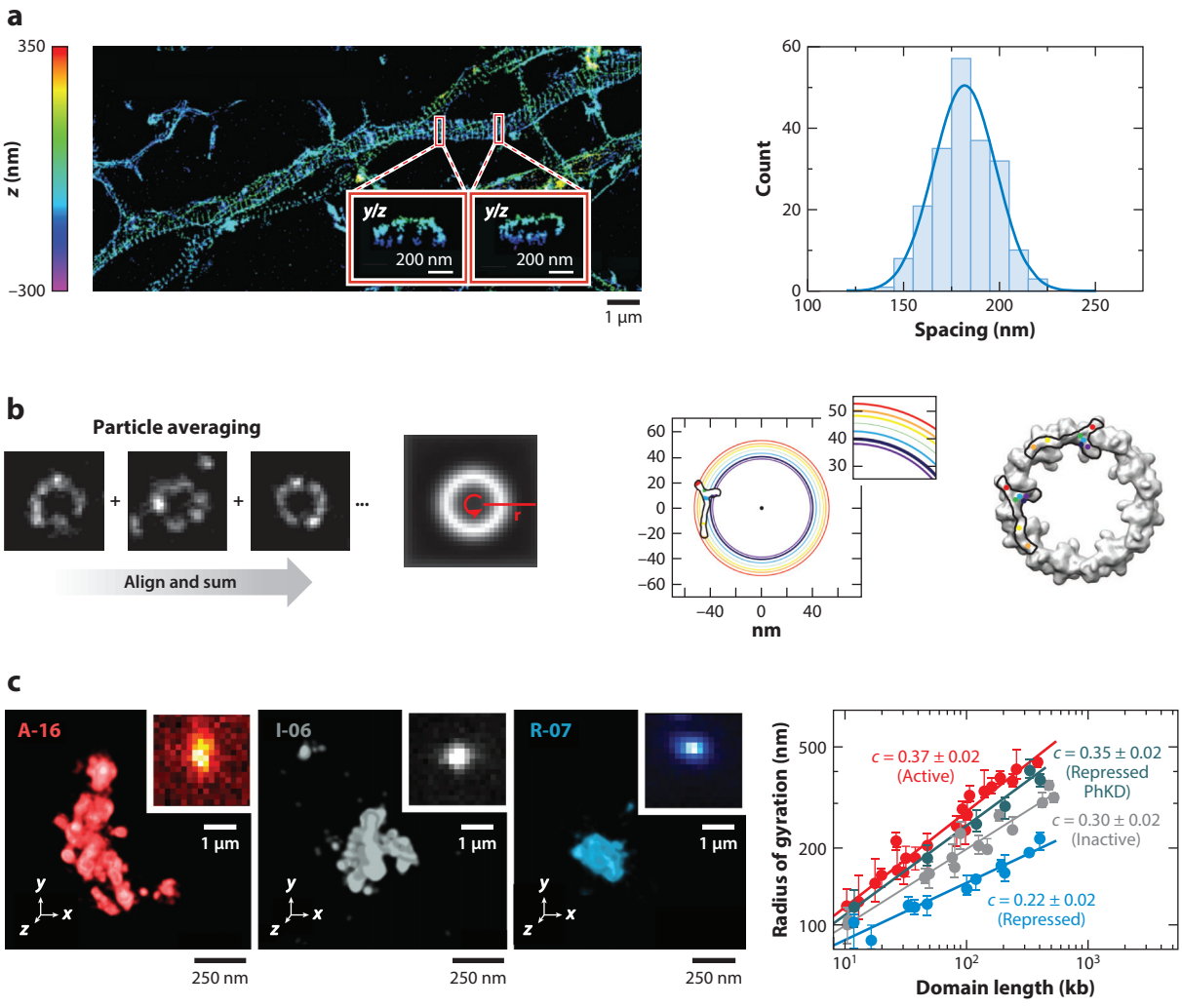

Figure 2

Examples of SMLM applications that have benefited from averaging and data reduction. (*a*) Spectrin rings in axons (*left*) are highly similar and can be shown to be periodic by projecting (averaging) orthogonally to the axis of the axon (*right*) (adapted from Reference 29 with permission). (*b*) Images of different nuclear pore y-complex subunits (*left*) can be aligned and averaged (*center*) to obtain standard radii for each subunit and to infer the orientation of the y-complex within the NPC (*right*) (adapted from Reference 31 with permission). (*c*) Despite considerable differences in structure, the reduction of gene–domain shape (*left*) to a single parameter, the radius of gyration, permits averaging and data analysis (*right*) (adapted from Reference 36 with permission). Abbreviations: NPC, nuclear pore complex; SMLM, single-molecule localization microscopy.

class of structures to image is not a reflection on the care and effort put into these publications but rather on what the method, in its current form, is best able to investigate.

2.2. More Complex Structures That Are Still Well Isolated

Structures that can still be well isolated, but have complex and variable structural features that do not allow for averaging, are somewhat harder to image and quantify than stereotyped structures.

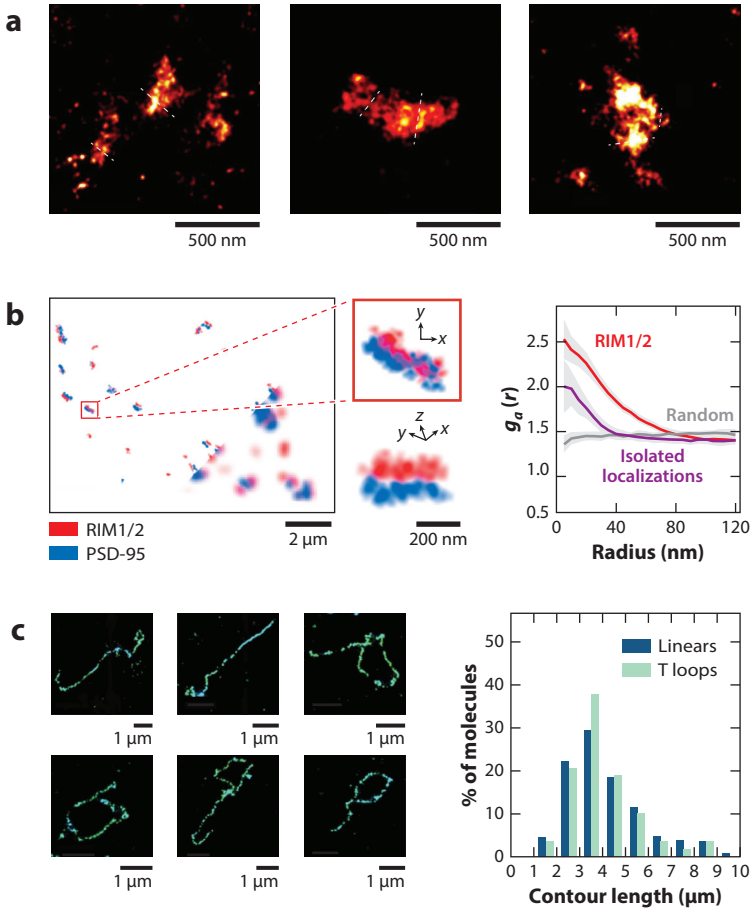

Figure 3

Examples of structures with variable structural features imaged by SMLM. (*a*) DNA-PAINT super-resolution images show the 174-kb hoxB locus in mouse embryonic fibroblasts (adapted from Reference 38 with permission). (*b*) Subsynaptic nanoclusters of synaptic proteins shown in an overview image (*left*) and zoom-in of the boxed synapse (*two center panels; shown from different angles*). By combining the data of many synapses, nanocluster sizes could be measured by calculating the autocorrelation functions (*right*) (adapted from Reference 40 with permission). (*c*) Examples of T loops after chromatin spreading (*left*) and the quantification of contour lengths for linear telomeric DNAs and telomeric T-loop DNA (*right*) are shown (adapted from Reference 43 with permission). Abbreviations: PAINT, points accumulation for imaging in nanoscale topography; SMLM, single-molecule localization microscopy.

This is the case, for example, when investigating the individual shape (rather than overall compactness) of individual gene loci (38) (**Figure 3*a***) or the local protein distribution in the active zone of individual synapses (39, 40) (**Figure 3*b***).

The need to extract high-quality information from individual objects, rather than an ensemble, means that each object must have a high density of localizations. Achieving high localization densities remains, however, very difficult. Current labeling chemistries, be it antibodies, SNAP, CLIP, or Halo tags (41, 42), or direct fusion proteins, label only a fraction of the target, and dye photochemistry further limits the portion of the labels one can actually see. As a result, the average distance between neighboring localizations is often of the same order of magnitude as

Localization precision: precision with which a single molecule can be localized

the feature size of interest. The statistical nature of the spatial distribution of localizations (see Section 4.4) can lead to the random formation of intriguing spatial arrangements and make it very tempting to overinterpret the images. Extraordinary scrutiny involving careful controls and statistical tests is therefore required for a reliable interpretation of the super-resolution images. Choosing effective quantitative descriptions, ideally informed by a hypothesis to be tested, can be a strategy to reduce the requirements for data quality and quantity. Unfortunately, these descriptions can often be quite abstract and the results less striking or intuitive than those for the first class, in which the repetitive nature of structures often allows a clear visual answer.

Owing to these difficulties, the existing studies that fall into this category are less numerous than those involving easily stereotyped structures. Clever tricks, however, can sometimes be applied to overcome some of the problems to get a clearer result. One example is a recent study on telomeric T loops in which the telomeric structure was simplified by spreading the chromatin to get an unambiguous readout of looping frequency (43) (**Figure 3*c***).

2.3. Complex and Closely Spaced Structures

The hardest class of structures to image are arguably those that either are not easily distinguishable from background or neighboring structures, or are extended and complex with features of interest in the 10- to 50-nm range. Examples include the Golgi complex in typical mammalian cells or chromatin in the interphase nucleus. These structures test the limits of localization microscopy, needing both exceptionally high labeling density and localization precision. If the required high labeling density is achieved, the fact that structures are extensive or not isolated means that every probe molecule is surrounded by large numbers of other probe molecules. The presence of large numbers of neighboring molecules adds additional requirements for exceptionally good photophysical or chemical control of the blinking characteristics. Otherwise, excessive overlap between the images of neighboring emitters prohibits localization of the emitters (resulting in black holes in the super-resolution image in areas of high labeling density) (44) or, in slightly less dense regions, leads to mislocalizations in which events do not appear in their true location (45, 46). An illustration of density-induced artifacts can be seen in **Figure 4**.

Hypothetical biological questions that would fall into this category include: counting microtubule valency in neuronal processes in which large bundles of microtubules run in parallel, identifying individual chromatin fibers in the interphase nucleus, isolating individual synaptic vesicles in presynaptic nerve terminals, and separating individual Golgi cisternae. To date, very few publications have tried to apply SMLM approaches to this class of structures. Those that come close have not achieved the ~30-nm resolution typical of SMLM and have been limited to reasonably qualitative results. For example, in our studies of amyloid plaques in primary mouse brain tissue (47), we were able to show differences in plaque compactness in response to TREM2 knockdown but were unable to reliably resolve individual filaments (**Figure 5*b***). With considerable care, it has been possible to resolve microtubules within small bundles in cultured cells (48); however, larger bundles in the same images remain unresolved, and taking this task into a tissue context remains an open challenge (**Figure 5*a***).

Super-resolution imaging of these classes of structures will benefit from substantial improvements in two areas. First, on the experimental side, the development of dyes, labeling approaches, and imaging schemes will result in better photophysical blinking properties and allow better control of the density of emitters. We consider PAINT and related techniques to have significant promise here. Second, the utilization of significant amounts of prior knowledge in image interpretation—for example, building microtubule diameters and persistence lengths into the analysis of microtubule bundles—may allow the requirements on labeling density to be somewhat

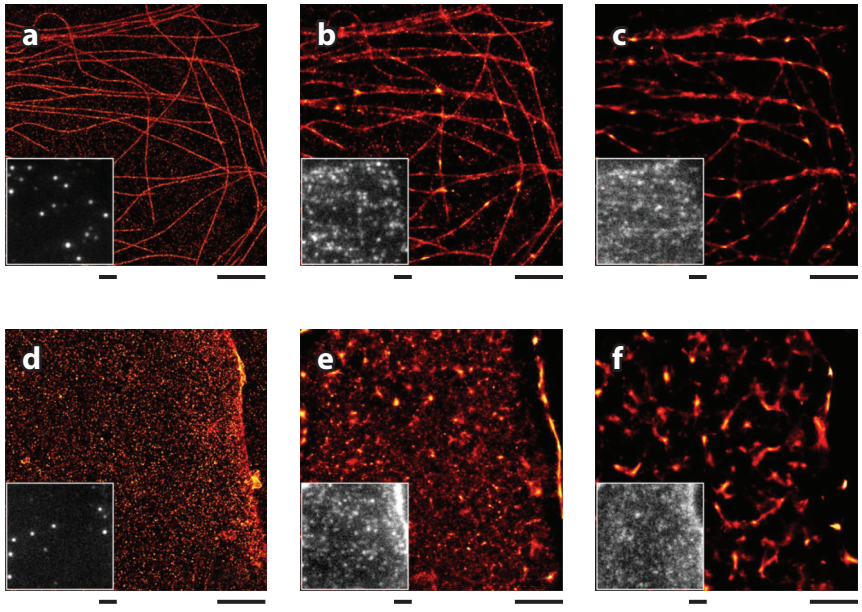

Figure 4

The ability to separate individual emitters in the raw data (*insets*) is crucial for accurate SMLM: Artifacts occur in areas of the image where imaging conditions do not allow for a sufficiently sparse emitter density. In particular, suitably low instantaneous blinking densities are hard to achieve for complex, extended structures. The blinking density increases from panels *a* to *c* (immunolabeled microtubules in a U2OS cell) and from panels *d* to *f* (WGA-labeled glycans on basal plasma membrane of a U2OS cell). Figure adapted from Reference 46 with permission. Scale bars = 2 μm. Abbreviations: SMLM, single-molecule localization microscopy; WGA, wheat germ agglutinin.

relaxed, albeit with an output that will more closely resemble a statistical test of a specific biological hypothesis than a conventional microscope image. Other strategies for dealing with highly complex structures include the extraction of simple, image-independent metrics such as pairwise-distance distributions between localizations and comparing them with rigorous simulations.

3. IMAGING INTERACTIONS

The second major category of questions addressed by SMLM focuses on interactions. For these questions, structure is only a secondary concern, potentially defining the environment in which the interactions take place. Interactions can be observed in a number of different ways, ranging from detecting clustering of a single species (49–53) (**Figure 6*a***) or coclustering of multiple species (54) to more conventional colocalization studies (55). While resolving structures is less important for these questions, SMLM can take advantage of its resolution, which is much closer to the size scales of molecular interactions than the diffraction-limited resolution of conventional light microscopy.

The (usually well-justified) hypothesis underlying the investigation of interactions is that molecular interactions come in discrete states: Either there is an interaction between two molecules or there is not. In more complex scenarios, a small number of additional, but still discrete, states is assumed. A typical analysis of interactions beyond the superficial level involves some form of classification into interacting and noninteracting pools of molecules. This classification may take

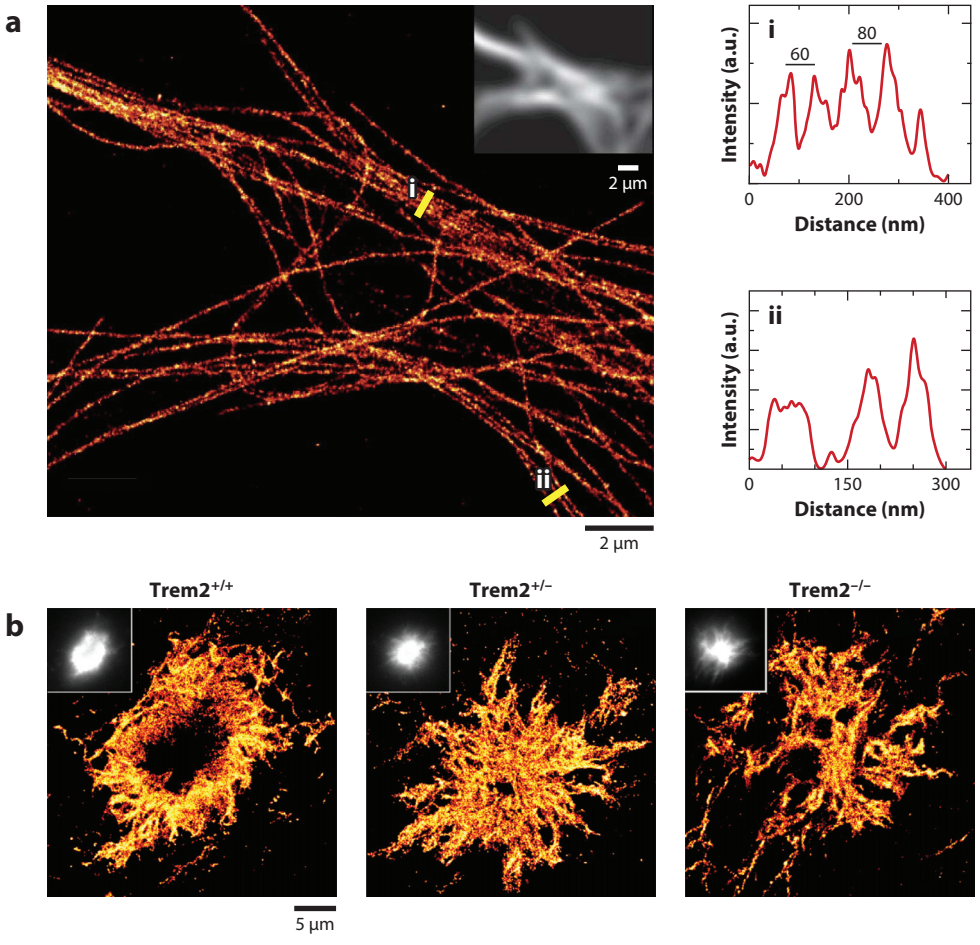

Figure 5

Resolving closely spaced or complex structures such as microtubule bundles (*a*) or amyloid plaque in tissue (*b*) is difficult. While close-to-ideal conditions permit microtubule bundles to be resolved along the profiles in panel *a* (*i*, *ii*), this is not possible in areas of the image such as the upper right, where microtubules are more closely spaced or cross each other in 3D. Similarly, in panel *b*, where the structure is complex and 3D, it was not possible to resolve individual amyloid fibrils. Quantification of complex structures is also typically more qualitative than in the simpler case, and to compare the effect of TREM2 knockdown in panel *b* we resorted to classifying image areas as "dense," "fibrillar," or "diffuse" and measuring the relative frequency of occurrence. Figure adapted from References 47 and 48 with permission.

the form of choosing the parameters of a clustering algorithm (see Section 5.2) or thresholding reconstructed images to perform colocalization analysis (see Section 5.3).

For example, by taking advantage of cluster analysis in two-color SMLM and counting localizations per cluster [as well as other techniques including fluorescence (Förster) resonance energy transfer (FRET) imaging], it could be shown that subunits of asialoglycoprotein receptors can assemble into homo- and hetero-oligomeric complexes that differ in ligand specificity and that the mix of the different types of complexes shows remarkable plasticity (56). For the more complex structure of cardiac ryanodine receptor (RyR) patches in rat ventricular myocytes, the level and spatial distribution of colocalization with junctophilin-2 (JPH2) could be determined from

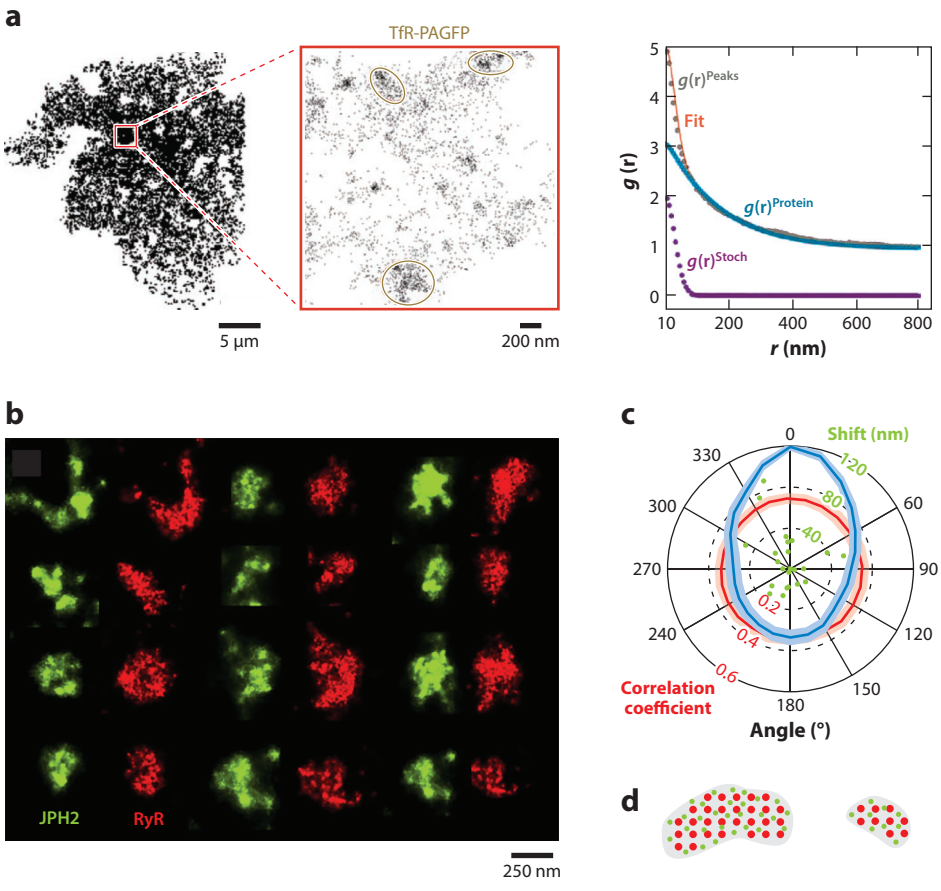

Figure 6

Examples of SMLM imaging of protein interactions. (*a*) Correlation analysis of PAGFP-labeled transferrin receptor located in the plasma membrane of a COS-7 cell reveals clustering of transferrin receptors (panel *a* adapted from Reference 51 with permission). (*b*) Data (examples shown *left*) of JPH2 (*light green*) and corresponding RyR (*red*) clusters were used to calculate Pearson's correlation (*c*) as a function of angular alignment of JPH2 in relation to corresponding RyR clusters (*blue*) and randomly chosen RyR clusters (*red*). These calculations resulted in a model (*d*) of the distribution of JPH2 (*light green*) in RyR (*red*) clusters (panels *b–d* adapted from Reference 57 with permission). Abbreviations: JPH2, junctophilin-2; PAGFP, photo-activatable green fluorescent protein; RyR, ryanodine receptor; SMLM, single-molecule localization microscopy.

two-color SMLM data by measuring the intensity of the JPH2 signal with respect to the boundary of RyR clusters, which was identified by thresholding (57) (**Figure 6*b***).

Instead of extracting information about interactions from fixed, static samples, looking for changes in dynamics of molecules in different states of interaction can often be an easier, more direct approach. Single-particle tracking is closely related to SMLM with many of its algorithms having acted as the basis of SMLM data analysis. Particle tracking allows a large range of different analyses such as the grouping of particle trajectories into trapped and diffusive populations or segments. Given the extensive history of this field, we refrain here from a detailed discussion and refer to a number of excellent reviews in this area (58–60). In the context of SMLM, however, we want to mention single-particle tracking PALM (sptPALM) (61–63), which allows individual

molecules to be followed even in scenarios of high molecular density by combining particle tracking with photoactivatable fluorescent markers.

4. THE COMPLEX QUESTION OF RESOLUTION

SMLM differs significantly from more conventional microscopy techniques in that there is no longer one clear concept or definition of resolution that is analogous to Abbe's simple function of wavelength and numerical aperture that applies to diffraction-limited systems (64). The resolving power is instead a function of a large number of parameters, several of which depend on the sample itself and vary from experiment to experiment. Two key concepts that underlie resolution in SMLM are the localization precision and the localization density. Ultimately, however, the concept of resolution might even depend on what one is trying to determine from the sample.

4.1. Localization Precision

Localization precision describes how well one can localize a single molecule. This depends on the underlying diffraction-limited resolution of the microscope, the number of photons one can collect from each molecule, camera properties, and the level of background signal. Localization precision has been extensively studied in the field of single-particle tracking (65) and can be determined through the calculation of the Cramer-Rao lower bound (CRLB), a formalism based on analyzing how fast the likelihood of getting a given image changes as the position of the molecule changes (66). For the special case of an approximately Gaussian-shaped PSF, localization precision can be estimated as (67):

$$\Delta x^2 = \frac{\sigma^2 + a^2/12}{N}\left(1 - 4\tau + \sqrt{\frac{2\tau}{1 + 4\tau}}\right),$$

where $\tau = \frac{2\pi b(\sigma^2 + a^2/12)}{N a^2}$, N is the number of signal photons, σ is the standard deviation of the PSF, a is the pixel size, and b is the number of background photons per pixel. A less complex, yet also less precise, estimate had been proposed earlier by Thompson and colleagues (65) and was corrected by Mortensen et al. (68).

It should be noted that CRLB analysis provides a theoretical lower bound on localization precision. The CRLB is estimated solely from the shape of the PSF and the signal and noise levels and assumes that the localization algorithm makes optimal use of the available image data. Additional influences such as drift and vibrations of the microscope, optical aberrations, or polarization effects that are not accounted for in the PSF are ignored, as are imperfections in the localization algorithm. The actual localization precision achieved will therefore always be worse and, in particular, depends strongly on the choice of localization algorithm. In practice, both maximum likelihood (ML) and suitably weighted least squares algorithms will get very close to the CRLB if allowed to converge. Centroid-based algorithms are significantly worse (65). Some care is needed when using iteration-limited ML (as in many GPU-based fitting approaches), as convergence is no longer guaranteed, and when using weighted least squares in cases in which the signals, background, and read noise are extremely low.

Localization precision is usually expressed as a 1-σ error in the estimated molecule positions. If we assume a Gaussian spread of errors, this translates into a full width at half-maximum (FWHM) of the distribution of localization errors of $\Delta x \approx 2.35\sigma$, which, in analogy to the FWHM of the PSF in conventional microscopy, can be used as a lower bound on the resolution. For example, a localization precision of 12 nm means that the resolution in a reconstructed image will be no better than 28 nm. The effect of varying localization precision can be seen in **Figure 7*a***.

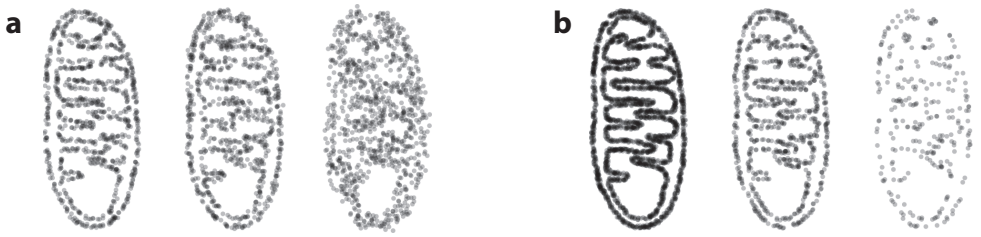

Figure 7

The effect of varying (*a*) localization precision and (*b*) localization density in the example of a simulated mitochondrion image. There is a 3-fold change in precision or density between neighboring images in panels *a* and *b*, respectively.

4.2. Localization Density

Localization density is the second major determinant of image resolution and, arguably, both the more important and the less well-understood one. It describes how many localizations were observed within a certain region of the image and is affected by both the density of the labeling and the switching properties of the sample (which is a function of both the fluorescent probe and the buffer/environment). At its most basic level, the concept boils down to the fact that one cannot separate two objects if one of them has not been observed. The relationship between localization density and resolution is, however, complex.

The Nyquist sampling criterion describes which spatial frequencies can be reconstructed when taking regularly spaced real values from a signal; however, the criterion is inadequate in SMLM, as localizations are not samples in the classical sense but rather are events that are neither regularly spaced nor have a value (other than 1) associated with them. Empirically, it seems that for a given resolution the distance between neighboring localizations should be significantly less than that indicated by a naive application of the Nyquist limit, with a factor of five times higher sampling having been proposed (69, 70). The effect of varying localization density can be seen in **Figure 7*b***.

4.3. Fourier Ring Correlation

Fourier ring correlation (FRC), or Fourier shell correlation in its three-dimensional version, was initially developed for electron microscopy (71) and is a method of measuring resolution in SMLM that attempts to quantify resolution by comparing two independent images of the same object (72, 73). The advantage of the technique is that it does not require any explicit knowledge of the imaging modality. The principle behind FRC is that frequency components within the two images that are above the noise floor (i.e., which can be resolved) will be correlated, but frequency components that are dominated by noise will not be correlated. By plotting correlation as a function of spatial frequency, one can determine at which spatial frequency the image content falls below a certain level.

The method has the considerable advantages that only two independent images of the same object are needed (which can be obtained in SMLM by randomly partitioning the acquired localizations into two sets) and that the method is sensitive to localization precision as well as density. Disadvantages stem from the fact that FRC curves depend on the shape of the imaged object since FRC implicitly measures the power spectrum of the object (i.e., how self-similar it is at different length scales). Images dominated by complex, extended objects can yield much worse FRC resolution values than images primarily containing small clusters scattered across the field of view. Especially when comparing experimental conditions for equivalent structures (e.g.,

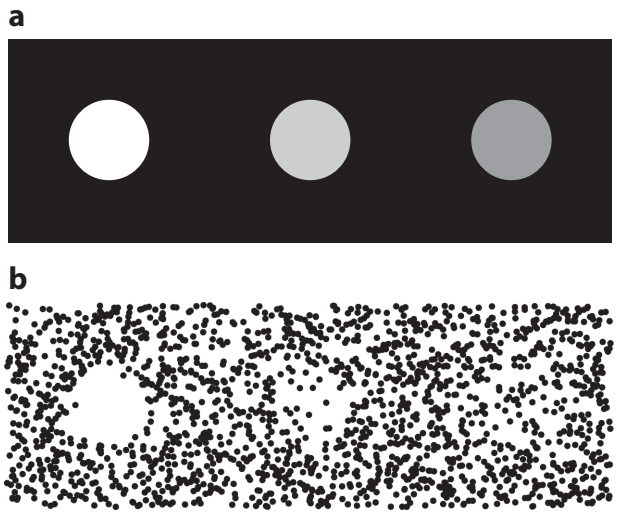

Figure 8

The basis of the Rose criterion is to assess the ability to distinguish a darker circle from bright background as a function of contrast under photon-starved conditions, as shown in panel *a*. Panel *b* shows synthetic photons (or equivalently localizations) for three circles of the same size but differing contrast. For a detailed discussion, see Rose (74).

similarly distributed microtubules at the cell periphery), FRC can be a very useful measure. It can be misleading, however, when used as a general purpose resolution estimate.

4.4. Stochastic Noise and Resolution

The resolution of conventional fluorescence microscopes is usually described by the shape of their PSF, as determined by objective choice and the diffraction of light (64). Although noise in the form of intensity variations in the image can conceal subtle features and thereby decrease the effective resolution in conventional microscope images, this effect is only significant for the dimmest of images and is usually ignored.

In contrast, SMLM approaches are much noisier and the influence of noise has to be considered. As discussed in Section 4.1, photon noise in the raw data implies a fundamental limit on the accuracy with which a single molecule can be localized. Additionally, and arguably more importantly, the stochastic process with which single molecules are labeled, switched, and detected represents a significant source of noise. The process of stochastic detection and localization is analogous to that of conventional imaging in exceptionally photon-starved conditions. The concept of resolution in photon-starved imaging was investigated in some detail in the somewhat unexpected context of image recording for television (74), resulting in the signal-to-noise ratio (SNR)–based Rose criterion for being able to detect a dark spot of low density on a uniform background of higher density (**Figure 8**):

$$d = \frac{5}{C\sqrt{n}}.$$

Here, d is the diameter of the smallest resolvable spot, n is the areal density of photons in the background (localizations if applied to SMLM imaging), and C is the contrast $[(n - n_{\text{spot}})/n < 1]$ between that spot and the background. While the Rose criterion is derived for the case of a darker

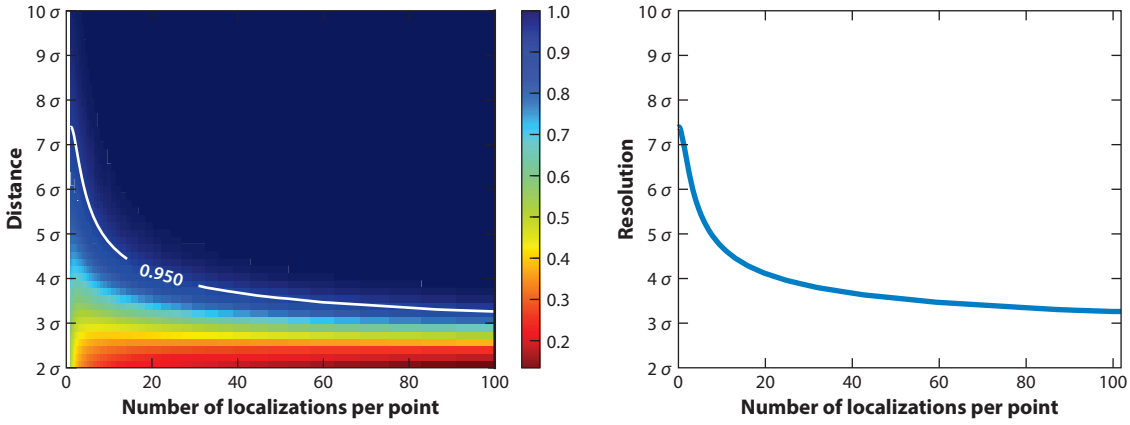

Figure 9

One can calculate the probability of observing a dip between two point objects as a function of their separation (in units of the localization precision σ). Significantly more localizations are required than would be expected from the Nyquist sampling criterion. For a 95% significance cutoff, the 2.35 σ resolution predicted by localization precision alone is achieved only in the limit of extremely high ($\gg$100) localization numbers.

spot on a brighter background, the concept (if not the scaling factor) that effective resolution is a function of both SNR (here in the form of the statistical counting SNR $\frac{n}{\sqrt{n}} = \sqrt{n}$) and contrast is expected to be equally applicable to SMLM. Rose's analysis and explanation is both well written and surprisingly relevant to our field. It is well worth a read if you can find a copy.

4.5. Combining Localization Precision and Density

Building on Rose's analysis, modeling less than infinite localization density as being a source of noise is one avenue toward a unified treatment of localization precision and localization density. Drawing on the Sparrow criterion, an empirical resolution metric used extensively in spectroscopy that defines two points as being resolved if there is a dip in signal between them (75, 76), one can derive an effective two-point resolution criterion for SMLM that takes localization density into account. The Sparrow criterion is easily extended to quantifying whether or not we can statistically detect a dip between two points considering the stochastic nature of localizations. The result is an expression for the probability of resolving two points as a function of their distance (as a multiple of the localization precision) and the number of localizations in each point, as illustrated in **Figure 9**.

Both this analysis and the Rose criterion imply that sampling should be much higher than naive application of the Nyquist limit, consistent with, or potentially exceeding, the 5-fold oversampling that has been put forward previously on a more empirical basis (69, 70).

4.6. Hypothesis Testing Instead of Resolution?

Our attempt at quantifying the two-point resolution is based on the probability of being able to separate two point-like objects. Resolving two points is a specialized example of a task one might wish to perform with SMLM. Other tasks—for example, detecting the unlabeled lumen within the membrane-labeled endoplasmic reticulum or a microtubule—can be accomplished with a significantly lower areal localization density. Conversely, if the phenomenon to be detected is very rare, higher densities could be required. Given these factors, we suggest that a hypothesis

testing approach in which one quantifies the ability to answer a specific question might be more useful and more tractable than a simple resolution figure.

The exact form that such a hypothesis test might take would vary substantially depending on the question at hand, as would the desirability of rigorously developing and performing such a test. Many applications may not need a rigorous definition of resolution, with the ultimate test being whether a difference in some high-level derived measure can be detected between two different experimental manipulations. A key advantage of this kind of resolution analysis would be to inform experimental planning by indicating what localization precision and density are required to answer a given question, which in turn would motivate the choice of dyes, labeling strategies, and illumination modalities. In the absence of a reasonably easy analytical approach to determine these values, a similar goal can be accomplished with the aid of simulations.

Regardless of how resolution is quantified, two key features become apparent: Resolution in SMLM is inherently a function of the structure being imaged as well as of the microscope, and labeling density is critical—most likely more so than previously appreciated.

5. QUANTIFYING MOLECULAR DISTRIBUTIONS

5.1. Counting Molecules

The fact that SMLM images are assembled from discrete localizations had sparked the idea already in the early days of SMLM to count the targeted molecules. In combination with the high spatial resolution provided by the imaging technique, this allows, in principle, measurement of important quantities such as the number of receptors associated with a vesicle or how many copies of a nucleoporin are part of an NPC. However, this seemingly straightforward task is in practice prone to many pitfalls and artifacts and requires careful calibrations and controls to obtain reliable results. The problem is that the number of observed localizations does not translate one-to-one into copy numbers of the molecule of interest. When extrinsic labeling techniques such as antibodies, PAINT labels, or dyes binding to SNAP or Halo tags (41, 42) are used, not every target molecule is labeled. Similarly, for genetically encoded tags, untagged copies of the molecule of interest (or molecules where the tag domain has not folded properly) might coexist with properly labeled molecules, or expression levels might differ from the original version. In contrast to genetically encoded tags, antibodies are in most cases labeled by more than one fluorophore. An additional source of error comes from the fact that some fluorescent probes might bleach before they can be detected, or they blink multiple times and are mistaken for multiple target molecules (77, 78). The combination of overcounting and undercounting errors related to these factors results in a hard-to-determine difference between the actual number of molecules and the obtained localization counts. A careful characterization and quantification of any of these effects can allow the introduced errors to be corrected (39, 79–86).

Much simpler is the task to obtain relative, rather than absolute, copy numbers and compare the numbers for different related proteins or for one protein under different physiological conditions. Many of the error sources in counting cancel out this way, which can reduce the number of required calibration steps significantly. Additionally, if for one of the samples the absolute number is known from other studies (e.g., biochemical assays or electron tomography), this number can be used for an internal calibration that translates the obtained relative copy numbers into absolute numbers (37, 87).

Given the complexity of the involved protocols and the large number of potential error sources, caution is advised, however, in following through with any of these approaches. Many of the mentioned factors are not well understood and can also be influenced by the microenvironment,

which can differ significantly between individual molecules. Furthermore, the relationship between localization counts and molecule counts is not strictly linear. At high molecular densities, for example, the algorithms are less likely to correctly identify each blinking event than they are for sparser distributions, and neighboring fluorescent probes can influence each other's photokinetics, leading to a different blinking behavior. All these potential problems therefore need to be factored into the experiments.

Segmentation: process of separating an image (or the underlying localizations) into areas belonging to objects of interest and areas representing background

5.2. Cluster Analysis and Segmentation

As seen by the examples provided in Sections 2 and 3, many of the molecules imaged by SMLM are clustered into 5- to 100-nm large functional units. The analysis of clustering and cluster sizes has therefore seen considerable interest in the field, and a number of statistical methods have been developed that quantify clustering directly from the molecule position data.

The first major advance related to clustering molecule position data was the use of the Ripley's K and related statistics, borrowed from the geosciences (50, 88, 89). These methods are based on the analysis of pairwise distances between all molecules. The Ripley's K statistic calculates the average number of molecules within a ring of given radius r from a molecule. If the distribution of molecules was random, one would expect the number of molecules in the ring to scale with its area (i.e., with r^2 in the two-dimensional case). Clustering is detected as a departure from this trend, typically seen as an excess at small radii. Slightly easier to interpret than the Ripley's K curve is the detrended and variance-normalized Ripley's L curve (89), which allows the statistical significance of the departure from uniformity to be read straight from the graph. Ripley's curves and related approaches can also give information about cluster sizes, although the interpretation is difficult if clusters are not of constant size and shape.

As biological clusters are rarely tightly distributed or uniformly shaped, analyzing the distribution of cluster sizes typically requires the segmentation and analysis of individual clusters, a process that can be surprisingly tricky especially in the presence of significant background. Approaches to cluster segmentation fall into two main classes: approaches adopted from classical statistical clustering, which operate directly on the point data and distance metrics between the points [e.g., k-means, DBSCAN (density-based spatial clustering of applications with noise)] (39, 53, 90, 91), and less direct approaches based on creating an estimate of local point density and then thresholding this image. Within the latter category, density estimation methods based on tessellation (92, 93) give a more robust estimate of areal density than the Gaussian rendering method often used for display purposes.

The most appropriate segmentation method depends strongly on the specific application, and having made extensive use of both direct and indirect methods, we have not seen compelling evidence to suggest that direct methods perform better. One potential advantage of indirect methods is that the caveats of threshold selection are well known, whereas the effects of the parameters used in direct methods are often less well understood—particularly when applied by nonexpert users. Regardless of the segmentation method chosen, parameter selection is critical to robust performance. An exciting new approach to parameter estimation for clustering (94) samples the entire parameter space and uses Bayes' theorem to select the appropriate parameters a posteriori. We feel that methods such as these have great potential to improve segmentation robustness.

5.3. Colocalization

One of the most compelling arguments for fluorescence microscopy is the ability to image multiple different markers in the same sample. In conventional fluorescence microscopy, colocalization, typically quantified using either Pearson's or Manders' coefficients, is an incredibly popular if

not always easily interpreted tool for looking at the association between two labels (95). One can in principle apply the same mathematics to SMLM reconstructions, although we strongly believe that conventional colocalization measures have limited utility on super-resolution images. It is physically impossible for two targets to occupy the same space, meaning that on a molecular-length scale colocalization (as defined by Pearson's or Manders' coefficients) is zero (or negative) by definition. As the resolution approaches the molecular scale, one observes very low colocalization, regardless of the target. The second major issue one confronts when applying colocalization methods to SMLM images is the large degree of stochasticity observed in many techniques (see Section 4).

In attempting to make colocalization work for SMLM images, one first needs to identify what it is that one really wants to measure with colocalization. In conventional microscopy, colocalization is very often interpreted as being supportive of a functional relationship, or interaction between the two proteins, whether direct or indirect. If two proteins are involved in the same pathway, they can be assumed to be concentrated within the same compartment or structure within the cell. As with any chemistry, interactions are transitory, and an increased concentration within the immediate neighborhood is likely sufficient for a functional relationship. In diffraction-limited microscopy, one can safely argue that the distances over which species interact are significantly shorter than our resolution limit, but this is no longer the case in super-resolved images. Here one has to explicitly consider the length scale that is important for the biological question and ask, "How close is colocalized?"

For this reason, we find colocalization metrics that have distance built into them attractive. One such distance-aware method generalizes the concepts used in Ripley's K-based cluster analysis and calculates the distribution of pairwise distances between channels, rather than within a single channel (54, 96–99). This method has the advantage of working directly from the position data, although like single-channel Ripley's K, the interpretation is not completely trivial. An alternative approach segments one channel to define a mask, calculates a Euclidian distance map from the mask, and then plots the distribution of the second channel with respect to its distance from the border of the segmented objects in the first channel (57, 100). This method has the advantage that it is also applicable to most other microscopy methods (e.g., confocal and STED microscopy) and provides easily understandable quantitative information about how close two proteins or structures are. An example of a conclusion reachable using distance transform–based approaches would be that 90% of one species is within 50 nm of the other.

6. CONCLUSIONS

The development of super-resolution microscopy has opened a world below the 100-nm scale to light microscopy. Despite relatively simple underlying concepts and commercially available instruments, obtaining high-quality data is not trivial. Nevertheless, these techniques have led to spectacular cell biological discoveries as demonstrated above. What these success stories have in common are (*a*) a well-posed biological question that is addressable by SMLM—be it by the nature of the examined structure that lends itself favorably to a super-resolution investigation or by clever experimental design—and (*b*) careful data analysis that rules out artifacts and builds confidence in the data. We see these examples as role models that can serve as inspiration for future studies.

As we discussed in Section 2, not every structure can be imaged equally well by SMLM and not every morphological question can be answered equally easily. Before embarking on an imaging project, we therefore recommend a careful assessment of how one's biological question relates to the strengths and weaknesses of SMLM, for example with the help of **Table 1**. This assessment allows one to develop a better understanding of the expected difficulty and obstacles, identify the

Table 1 Structural attributes and their consequences to data quality and processing

Structural attribute	Example(s)	Consequence(s)
Positive attributes		
Structures can be easily distinguished from surroundings	Cilia (34) Needle complex in bacteria (87)	Structures can be isolated from neighboring structures and background
Known geometrical constraints	Microtubules Actin rings in axons (29)	Modeling can be applied Reduces requirements for localization density
Stereotypical features	Nuclear pore complex (31, 32) Bacteriophages (35)	Population averaging can often be applied Reduces requirements for localization density
Two-dimensional	Clusters in plasma membrane (56)	Third dimension can be neglected
Structure can be described with a simple parameter	Diameter of cytokinesis nodes (37) Radius of gyration of gene loci (36)	Fewer localizations required to extract parameter than fully characterize object Parameter of interest can be averaged over multiple samples
Challenging attributes		
Bulky three-dimensional structure	Golgi complex Chromatin in interphase nucleus Actin in muscle cells	Difficult to achieve sparse blinking conditions that allow reliably localized molecules High localization densities required to identify features in complex architecture Potential issues with epitope accessibility or labeling efficiency
Highly variable structure	Amyloid plaque (47)	Difficult to find simplifying measures Analysis more qualitative
Fast dynamics	Transferrin receptor movement on plasma membrane (110)	Short recording times required Number of recorded frames per image limited Compromise between localization density and motion artifacts
Low target molecule density	Some organelle or plasma membrane proteins Rare histones or histone modifications	Resulting low localization density limits resolution Poor representation of underlying organelle
Densely labeled, subdiffraction-sized structures	Peroxisomes P-bodies	Cannot easily recognize artifacts due to multiple simultaneous emitters Incorrect size measurements
High background	Tissue Out-of-focus fluorescence (e.g., around the nucleus) Large cytoplasmic pool of labeled protein	High localization densities required to achieve statistical significance in structural interpretation Difficult to segment structure

required controls, and align expectations of what the quantifiable outcome of the project will be. In turn, this assessment provides an opportunity to adjust the experimental design early on in the project to take best advantage of the available super-resolution imaging and analysis tools.

Performing such an assessment is, of course, well established for many biological techniques for which the complexity of the experiment and the abstractness of the acquired data require careful planning. When using conventional microscopy, however, an image is taken quickly and the result is often intuitively interpretable, making rigorous preliminary assessment and design much less critical. This approach does not transfer well to SMLM, and the first step in successful super-resolution imaging is the appreciation of the complexity of the method and the numerous pitfalls that have to be avoided.

Fortunately, as we indicated in this review, more and better tools that assist with the design and analysis of localization microscopy experiments become available at a breathtaking speed. In addition to better analysis algorithms, which we discussed in Sections 4 and 5, our understanding of fluorescent probes' photophysical properties is increasingly better. For example, data on the number of blinking events of mEos2 (79); the photoactivation efficiency of a number of photoswitchable fluorescent proteins (101); or the ON fraction, ON time, and number of detected photons per Alexa 647 molecule at different laser intensities (102) are now available. Data like these can be used in simulators (103, 104) that provide a preview of the expected data quality and provide numerical controls in which the ground-truth structure put into the simulator can be compared with the super-resolution image obtained from the simulation that mimics the imaging process.

Additionally, we continue to witness exciting developments of new probes (105), better imaging buffers (12, 106, 107), and innovative illumination schemes (70, 108) that improve the quality of the raw data in an increasing range of applications. Developments toward better live-cell SMLM are particularly promising (109–111). Although most of the examples we have presented in this review have been on fixed cells, the same considerations can be applied to live-cell SMLM, albeit with an additional constraint on the recording speed and the problem that available localizations need to be divided among the reconstructed images of the recorded time lapse sequence.

Projecting from current developments in SMLM into the future, we expect a continuing improvement in the community's understanding of the constraints and dependencies of this microscopy modality that will lead to increasingly reliable, quantitative data. Automation of the imaging and analysis processes combined with speed increases in both areas will allow higher throughput in SMLM and will enable the detection of more subtle and/or rare phenomena than have been demonstrated to date. With these developments, and analogous developments in other super-resolution techniques like STED microscopy, super-resolution microscopy as a whole will continue to expand its application range and has, in our opinion, the potential to replace conventional light microscopy in subcellular imaging questions as the dominant go-to technique.

DISCLOSURE STATEMENT

J.B. discloses significant financial interest in Bruker Corporation and Hamamatsu Photonics that might be perceived as affecting the objectivity of this review.

ACKNOWLEDGMENTS

D.B. and J.B. have received funding from the National Institutes of Health (U01 EB021232, R01 GM118486, P30 DK045735), the G. Harold and Leila Y. Mathers Foundation, and the Wellcome Trust (203285/B/16/Z). We would also like to thank Andrew Barentine, Kenny Chung, Kevin Hu, Zach Marin, and Mengyuan Sun for their help in proofreading the manuscript and constructive suggestions.

LITERATURE CITED

1. Van Norden R. 2014. Nobel for microscopy that reveals inner world of cells. *Nature* 514:286
2. Hirano Y, Matsuda A, Hiraoka Y. 2015. Recent advancements in structured-illumination microscopy toward live-cell imaging. *Microscopy* 64:237–49
3. Ströhl F, Kaminski CF. 2016. Frontiers in structured illumination microscopy. *Optica* 3:667–77
4. Demmerle J, Innocent C, North AJ, Ball G, Muller M, et al. 2017. Strategic and practical guidelines for successful structured illumination microscopy. *Nat. Protoc.* 12:988–1010

5. Hell SW, Wichmann J. 1994. Breaking the diffraction resolution limit by stimulated emission: stimulated-emission-depletion fluorescence microscopy. *Opt. Lett.* 19:780–82
6. Bottanelli F, Kromann EB, Allgeyer ES, Erdmann RS, Wood Baguley S, et al. 2016. Two-colour live-cell nanoscale imaging of intracellular targets. *Nat. Commun.* 7:10778
7. Hell SW, Dyba M, Jakobs S. 2004. Concepts for nanoscale resolution in fluorescence microscopy. *Curr. Opin. Neurobiol.* 14:599–609
8. Dertinger T, Pallaoro A, Braun G, Ly S, Laurence TA, Weiss S. 2013. Advances in superresolution optical fluctuation imaging (SOFI). *Q. Rev. Biophys.* 46:210–21
9. Eggeling C, Willig KI, Sahl SJ, Hell SW. 2015. Lens-based fluorescence nanoscopy. *Q. Rev. Biophys.* 48:178–243
10. Huang B, Bates M, Zhuang X. 2009. Super-resolution fluorescence microscopy. *Annu. Rev. Biochem.* 78:993–1016
11. Patterson G, Davidson M, Manley S, Lippincott-Schwartz J. 2010. Superresolution imaging using single-molecule localization. *Annu. Rev. Phys. Chem.* 61:345–67
12. Sauer M, Heilemann M. 2017. Single-molecule localization microscopy in eukaryotes. *Chem. Rev.* 117:7478–509
13. von Diezmann A, Shechtman Y, Moerner WE. 2017. Three-dimensional localization of single molecules for super-resolution imaging and single-particle tracking. *Chem. Rev.* 117:7244–75
14. Betzig E, Patterson GH, Sougrat R, Lindwasser OW, Olenych S, et al. 2006. Imaging intracellular fluorescent proteins at nanometer resolution. *Science* 313:1642–45
15. Hess ST, Girirajan TP, Mason MD. 2006. Ultra-high resolution imaging by fluorescence photoactivation localization microscopy. *Biophys. J.* 91:4258–72
16. Rust MJ, Bates M, Zhuang X. 2006. Sub-diffraction-limit imaging by stochastic optical reconstruction microscopy (STORM). *Nat. Methods* 3:793–95
17. Heilemann M, van de Linde S, Schuttpelz M, Kasper R, Seefeldt B, et al. 2008. Subdiffraction-resolution fluorescence imaging with conventional fluorescent probes. *Angew. Chem. Int. Ed. Engl.* 47:6172–76
18. Folling J, Bossi M, Bock H, Medda R, Wurm CA, et al. 2008. Fluorescence nanoscopy by ground-state depletion and single-molecule return. *Nat. Methods* 5:943–45
19. Lemmer P, Gunkel M, Baddeley D, Kaufmann R, Urich A, et al. 2008. SPDM: light microscopy with single-molecule resolution at the nanoscale. *Appl. Phys. B* 93:1
20. Baddeley D, Jayasinghe ID, Cremer C, Cannell MB, Soeller C. 2009. Light-induced dark states of organic fluochromes enable 30 nm resolution imaging in standard media. *Biophys. J.* 96:L22–24
21. Sharonov A, Hochstrasser RM. 2006. Wide-field subdiffraction imaging by accumulated binding of diffusing probes. *PNAS* 103:18911–16
22. Flors C, Ravarani CNJ, Dryden DTF. 2009. Super-resolution imaging of DNA labelled with intercalating dyes. *ChemPhysChem* 10:2201–4
23. Jungmann R, Steinhauer C, Scheible M, Kuzyk A, Tinnefeld P, Simmel FC. 2010. Single-molecule kinetics and super-resolution microscopy by fluorescence imaging of transient binding on DNA origami. *Nano Lett.* 10:4756–61
24. Schoen I, Ries J, Klotzsch E, Ewers H, Vogel V. 2011. Binding-activated localization microscopy of DNA structures. *Nano Lett.* 11:4008–11
25. Lew MD, Lee SF, Ptacin JL, Lee MK, Twieg RJ, et al. 2011. Three-dimensional superresolution colocalization of intracellular protein superstructures and the cell surface in live *Caulobacter crescentus*. *PNAS* 108:18577–78
26. Burnette DT, Sengupta P, Dai Y, Lippincott-Schwartz J, Kachar B. 2011. Bleaching/blinking assisted localization microscopy for superresolution imaging using standard fluorescent molecules. *PNAS* 108:21081–86
27. Jungmann R, Avendano MS, Woehrstein JB, Dai M, Shih WM, Yin P. 2014. Multiplexed 3D cellular super-resolution imaging with DNA-PAINT and Exchange-PAINT. *Nat. Methods* 11:313–18
28. Hell SW. 2015. Nanoscopy with focused light (Nobel lecture). *Angew. Chem. Int. Ed. Engl.* 54:8054–66
29. Xu K, Zhong G, Zhuang X. 2013. Actin, spectrin, and associated proteins form a periodic cytoskeletal structure in axons. *Science* 339:452–56

30. Chung JJ, Shim SH, Everley RA, Gygi SP, Zhuang X, Clapham DE. 2014. Structurally distinct Ca(2+) signaling domains of sperm flagella orchestrate tyrosine phosphorylation and motility. *Cell* 157:808–22
31. Szymborska A, de Marco A, Daigle N, Cordes VC, Briggs JAG, Ellenberg J. 2013. Nuclear pore scaffold structure analyzed by super-resolution microscopy and particle averaging. *Science* 341:655–58
32. Loschberger A, van de Linde S, Dabauvalle MC, Rieger B, Heilemann M, et al. 2012. Super-resolution imaging visualizes the eightfold symmetry of gp210 proteins around the nuclear pore complex and resolves the central channel with nanometer resolution. *J. Cell Sci.* 125:570–75
33. Broeken J, Johnson H, Lidke DS, Liu S, Nieuwenhuizen RP, et al. 2015. Resolution improvement by 3D particle averaging in localization microscopy. *Methods Appl. Fluoresc.* 3:014003
34. Shi X, Garcia G III, Van De Weghe JC, McGorty R, Pazour GJ, et al. 2017. Super-resolution microscopy reveals that disruption of ciliary transition-zone architecture causes Joubert syndrome. *Nat. Cell Biol.* 19:1178–88
35. Huang F, Sirinakis G, Allgeyer ES, Schroeder LK, Duim WC, et al. 2016. Ultra-high resolution 3D imaging of whole cells. *Cell* 166:1028–40
36. Boettiger AN, Bintu B, Moffitt JR, Wang S, Beliveau BJ, et al. 2016. Super-resolution imaging reveals distinct chromatin folding for different epigenetic states. *Nature* 529:418–22
37. Laplante C, Huang F, Tebbs IR, Bewersdorf J, Pollard TD. 2016. Molecular organization of cytokinesis nodes and contractile rings by super-resolution fluorescence microscopy of live fission yeast. *PNAS* 113:E5876–85
38. Beliveau BJ, Boettiger AN, Avendano MS, Jungmann R, McCole RB, et al. 2015. Single-molecule super-resolution imaging of chromosomes and in situ haplotype visualization using Oligopaint FISH probes. *Nat. Commun.* 6:7147
39. Ehmann N, van de Linde S, Alon A, Ljaschenko D, Keung XZ, et al. 2014. Quantitative super-resolution imaging of Bruchpilot distinguishes active zone states. *Nat. Commun.* 5:4650
40. Tang A-H, Chen H, Li TP, Metzbower SR, MacGillavry HD, Blanpied TA. 2016. A trans-synaptic nanocolumn aligns neurotransmitter release to receptors. *Nature* 536:210–14
41. Los GV, Encell LP, McDougall MG, Hartzell DD, Karassina N, et al. 2008. HaloTag: a novel protein labeling technology for cell imaging and protein analysis. *ACS Chem. Biol.* 3:373–82
42. Keppler A, Gendreizig S, Gronemeyer T, Pick H, Vogel H, Johnsson K. 2003. A general method for the covalent labeling of fusion proteins with small molecules in vivo. *Nat. Biotechnol.* 21:86–89
43. Doksani Y, Wu JY, de Lange T, Zhuang X. 2013. Super-resolution fluorescence imaging of telomeres reveals TRF2-dependent T-loop formation. *Cell* 155:345–56
44. Huang F, Schwartz SL, Byars JM, Lidke KA. 2011. Simultaneous multiple-emitter fitting for single molecule super-resolution imaging. *Biomed. Opt. Express* 2:1377–93
45. Erdelyi M, Sinko J, Kakonyi R, Kelemen A, Rees E, et al. 2015. Origin and compensation of imaging artefacts in localization-based super-resolution microscopy. *Methods* 88:122–32
46. Burgert A, Letschert S, Doose S, Sauer M. 2015. Artifacts in single-molecule localization microscopy. *Histochem. Cell Biol.* 144:123–31
47. Yuan P, Condello C, Keene CD, Wang Y, Bird TD, et al. 2016. TREM2 haplodeficiency in mice and humans impairs the microglia barrier function leading to decreased amyloid compaction and severe axonal dystrophy. *Neuron* 90:724–39
48. Mikhaylova M, Cloin BM, Finan K, van den Berg R, Teeuw J, et al. 2015. Resolving bundled microtubules using anti-tubulin nanobodies. *Nat. Commun.* 6:7933
49. Baddeley D, Jayasinghe ID, Lam L, Rossberger S, Cannell MB, Soeller C. 2009. Optical single-channel resolution imaging of the ryanodine receptor distribution in rat cardiac myocytes. *PNAS* 106:22275–80
50. Owen DM, Rentero C, Rossy J, Magenau A, Williamson D, et al. 2010. PALM imaging and cluster analysis of protein heterogeneity at the cell surface. *J. Biophotonics* 3:446–54
51. Sengupta P, Jovanovic-Talisman T, Skoko D, Renz M, Veatch SL, Lippincott-Schwartz J. 2011. Probing protein heterogeneity in the plasma membrane using PALM and pair correlation analysis. *Nat. Methods* 8:969–75
52. Bar-On D, Wolter S, van de Linde S, Heilemann M, Nudelman G, et al. 2012. Super-resolution imaging reveals the internal architecture of nano-sized syntaxin clusters. *J. Biol. Chem.* 287:27158–67

53. Nan X, Collisson EA, Lewis S, Huang J, Tamguney TM, et al. 2013. Single-molecule superresolution imaging allows quantitative analysis of RAF multimer formation and signaling. *PNAS* 110:18519–24
54. Caetano FA, Dirk BS, Tam JHK, Cavanagh PC, Goiko M, et al. 2015. MIiSR: Molecular interactions in super-resolution imaging enables the analysis of protein interactions, dynamics and formation of multi-protein structures. *PLOS Comput. Biol.* 11:e1004634
55. Brown TA, Tkachuk AN, Shtengel G, Kopek BG, Bogenhagen DF, et al. 2011. Superresolution fluorescence imaging of mitochondrial nucleoids reveals their spatial range, limits, and membrane interaction. *Mol. Cell. Biol.* 31:4994–5010
56. Renz M, Daniels BR, Vamosi G, Arias IM, Lippincott-Schwartz J. 2012. Plasticity of the asialoglycoprotein receptor deciphered by ensemble FRET imaging and single-molecule counting PALM imaging. *PNAS* 109:E2989–97
57. Jayasinghe ID, Baddeley D, Kong CH, Wehrens XH, Cannell MB, Soeller C. 2012. Nanoscale organization of junctophilin-2 and ryanodine receptors within peripheral couplings of rat ventricular cardiomyocytes. *Biophys. J.* 102:L19–21
58. Triller A, Choquet D. 2008. New concepts in synaptic biology derived from single-molecule imaging. *Neuron* 59:359–74
59. Chenouard N, Smal I, de Chaumont F, Maska M, Sbalzarini IF, et al. 2014. Objective comparison of particle tracking methods. *Nat. Methods* 11:281–89
60. Kusumi A, Tsunoyama TA, Hirosawa KM, Kasai RS, Fujiwara TK. 2014. Tracking single molecules at work in living cells. *Nat. Chem. Biol.* 10:524–32
61. Manley S, Gillette JM, Patterson GH, Shroff H, Hess HF, et al. 2008. High-density mapping of single-molecule trajectories with photoactivated localization microscopy. *Nat. Methods* 5:155–57
62. Giannone G, Hosy E, Levet F, Constals A, Schulze K, et al. 2010. Dynamic superresolution imaging of endogenous proteins on living cells at ultra-high density. *Biophys. J.* 99:1303–10
63. Hoze N, Nair D, Hosy E, Sieben C, Manley S, et al. 2012. Heterogeneity of AMPA receptor trafficking and molecular interactions revealed by superresolution analysis of live cell imaging. *PNAS* 109:17052–57
64. Abbe E. 1873. Beiträge zur Theorie des Mikroskops und der mikroskopischen Wahrnehmung. *Arch. Mikrosk. Anat.* 9:413–68
65. Thompson RE, Larson DR, Webb WW. 2002. Precise nanometer localization analysis for individual fluorescent probes. *Biophys. J.* 82:2775–83
66. Ober RJ, Ram S, Ward ES. 2004. Localization accuracy in single-molecule microscopy. *Biophys. J.* 86:1185–200
67. Rieger B, Stallinga S. 2014. The lateral and axial localization uncertainty in super-resolution light microscopy. *ChemPhysChem* 15:664–70
68. Mortensen KI, Churchman LS, Spudich JA, Flyvbjerg H. 2010. Optimized localization analysis for single-molecule tracking and super-resolution microscopy. *Nat. Methods* 7:377–81
69. Li D, Shao L, Chen BC, Zhang X, Zhang M, et al. 2015. Extended-resolution structured illumination imaging of endocytic and cytoskeletal dynamics. *Science* 349:aab3500
70. Legant WR, Shao L, Grimm JB, Brown TA, Milkie DE, et al. 2016. High-density three-dimensional localization microscopy across large volumes. *Nat. Methods* 13:359–65
71. van Heel M, Gowen B, Matadeen R, Orlova EV, Finn R, et al. 2001. Single-particle electron cryomicroscopy: towards atomic resolution. *Q. Rev. Biophys.* 33:307–69
72. Nieuwenhuizen RP, Lidke KA, Bates M, Puig DL, Grunwald D, et al. 2013. Measuring image resolution in optical nanoscopy. *Nat. Methods* 10:557–62
73. Banterle N, Bui KH, Lemke EA, Beck M. 2013. Fourier ring correlation as a resolution criterion for super-resolution microscopy. *J. Struct. Biol.* 183:363–67
74. Rose A. 1973. *Vision: Human and Electronic*. New York: Plenum Press
75. Sparrow CM. 1916. On spectroscopic resolving power. *Astrophys. J.* 44:76–86
76. den Dekker AJ, van den Bos A. 1997. Resolution: a survey. *J. Opt. Soc. Am. A* 14:547–57
77. Annibale P, Vanni S, Scarselli M, Rothlisberger U, Radenovic A. 2011. Identification of clustering artifacts in photoactivated localization microscopy. *Nat. Methods* 8:527–28

78. Veatch SL, Machta BB, Shelby SA, Chiang EN, Holowka DA, Baird BA. 2012. Correlation functions quantify super-resolution images and estimate apparent clustering due to over-counting. *PLOS ONE* 7:e31457
79. Annibale P, Vanni S, Scarselli M, Rothlisberger U, Radenovic A. 2011. Quantitative photo activated localization microscopy: unraveling the effects of photoblinking. *PLOS ONE* 6:e22678
80. Coltharp C, Kessler RP, Xiao J. 2012. Accurate construction of photoactivated localization microscopy (PALM) images for quantitative measurements. *PLOS ONE* 7:e51725
81. Lee SH, Shin JY, Lee A, Bustamante C. 2012. Counting single photoactivatable fluorescent molecules by photoactivated localization microscopy (PALM). *PNAS* 109:17436–41
82. Puchner EM, Walter JM, Kasper R, Huang B, Lim WA. 2013. Counting molecules in single organelles with superresolution microscopy allows tracking of the endosome maturation trajectory. *PNAS* 110:16015–20
83. Rollins GC, Shin JY, Bustamante C, Pressé S. 2015. Stochastic approach to the molecular counting problem in superresolution microscopy. *PNAS* 112:E110–18
84. Fricke F, Beaudouin J, Eils R, Heilemann M. 2015. One, two or three? Probing the stoichiometry of membrane proteins by single-molecule localization microscopy. *Sci. Rep.* 5:14072
85. Nieuwenhuizen RP, Nahidiazar L, Manders EM, Jalink K, Stallinga S, Rieger B. 2015. Co-orientation: quantifying simultaneous co-localization and orientational alignment of filaments in light microscopy. *PLOS ONE* 10:e0131756
86. Hummer G, Fricke F, Heilemann M. 2016. Model-independent counting of molecules in single-molecule localization microscopy. *Mol. Biol. Cell* 27:3637–44
87. Zhang Y, Lara-Tejero M, Bewersdorf J, Galan JE. 2017. Visualization and characterization of individual type III protein secretion machines in live bacteria. *PNAS* 114:6098–103
88. Ripley BD. 1976. The second-order analysis of stationary point processes. *J. Appl. Probab.* 13:255–66
89. Dixon PM. 2006. In *Encyclopedia of Environmetrics*, pp. 1796–803. New York: John Wiley
90. Schubert E, Sander J, Ester M, Kriegel HP, Xu X. 2017. DBSCAN revisited, revisited: why and how you should (still) use DBSCAN. *ACM Trans. Database Syst.* 42:1–21
91. MacQueen J. 1967. *Some methods for classification and analysis of multivariate observations*. Vol. 1, Statistics. Presented at Proc. Fifth Berkeley Symp. Math. Stat. Probab., Berkeley, CA
92. Baddeley D, Cannell MB, Soeller C. 2010. Visualization of localization microscopy data. *Microsc. Microanal* 16:64–72
93. Levet F, Hosy E, Kechkar A, Butler C, Beghin A, et al. 2015. SR-Tesseler: a method to segment and quantify localization-based super-resolution microscopy data. *Nat. Methods* 12:1065–71
94. Rubin-Delanchy P, Burn GL, Griffie J, Williamson DJ, Heard NA, et al. 2015. Bayesian cluster identification in single-molecule localization microscopy data. *Nat. Methods* 12:1072–76
95. Dunn KW, Kamocka MM, McDonald JH. 2011. A practical guide to evaluating colocalization in biological microscopy. *Am. J. Physiol. Cell Physiol.* 300:C723–42
96. Lagache T, Sauvonnet N, Danglot L, Olivo-Marin JC. 2015. Statistical analysis of molecule colocalization in bioimaging. *Cytometry Part A* 87:568–79
97. Coltharp C, Yang X, Xiao J. 2014. Quantitative analysis of single-molecule superresolution images. *Curr. Opin. Struct. Biol.* 28:112–21
98. Rossy J, Cohen E, Gaus K, Owen DM. 2014. Method for co-cluster analysis in multichannel single-molecule localisation data. *Histochem. Cell Biol.* 141:605–12
99. Tarancón Díez L, Bönsch C, Malkusch S, Truan Z, Munteanu M, et al. 2014. Coordinate-based co-localization-mediated analysis of arrestin clustering upon stimulation of the C–C chemokine receptor 5 with RANTES/CCL5 analogues. *Histochem. Cell Biol.* 142:69–77
100. Veeraraghavan R, Gourdie RG. 2016. Stochastic optical reconstruction microscopy-based relative localization analysis (STORM-RLA) for quantitative nanoscale assessment of spatial protein organization. *Mol. Biol. Cell* 27:3583–90
101. Durisic N, Laparra-Cuervo L, Sandoval-Alvarez A, Borbely JS, Lakadamyali M. 2014. Single-molecule evaluation of fluorescent protein photoactivation efficiency using an in vivo nanotemplate. *Nat. Methods* 11:156–62

102. Lin Y, Long JJ, Huang F, Duim WC, Kirschbaum S, et al. 2015. Quantifying and optimizing single-molecule switching nanoscopy at high speeds. *PLOS ONE* 10:e0128135
103. Venkataramani V, Herrmannsdorfer F, Heilemann M, Kuner T. 2016. SuReSim: simulating localization microscopy experiments from ground truth models. *Nat. Methods* 13:319–21
104. Novak T, Gajdos T, Sinko J, Szabo G, Erdelyi M. 2017. TestSTORM: versatile simulator software for multimodal super-resolution localization fluorescence microscopy. *Sci. Rep.* 7:951
105. Zheng Q, Lavis LD. 2017. Development of photostable fluorophores for molecular imaging. *Curr. Opin. Chem. Biol.* 39:32–38
106. Hartwich TMP, Soeller C, Baddeley D. 2014. A simple chemical oxygen scavenging system for improved dSTORM tissue imaging. *Biophys. J.* 106:401a
107. Allen JR, Silfies JS, Schwartz SA, Davidson MW. *Single-Molecule Super-Resolution Imaging*. New York: Nikon Instruments. **https://www.microscopyu.com/techniques/super-resolution/single-molecule-super-resolution-imaging**
108. Cella Zanacchi F, Lavagnino Z, Perrone Donnorso M, Del Bue A, Furia L, et al. 2011. Live-cell 3D super-resolution imaging in thick biological samples. *Nat. Methods* 8:1047–49
109. Jones SA, Shim SH, He J, Zhuang X. 2011. Fast, three-dimensional super-resolution imaging of live cells. *Nat. Methods* 8:499–508
110. Huang F, Hartwich TM, Rivera-Molina FE, Lin Y, Duim WC, et al. 2013. Video-rate nanoscopy using sCMOS camera-specific single-molecule localization algorithms. *Nat. Methods* 10:653–58
111. Takakura H, Zhang Y, Erdmann RS, Thompson AD, Lin Y, et al. 2017. Long time-lapse nanoscopy with spontaneously blinking membrane probes. *Nat. Biotechnol.* 35:773–80